Applied Catalysis B: Environmental 115–116 (2012) 294–302

Contents lists available at SciVerse ScienceDirect

Applied Catalysis B: Environmental

journal homepage: www.elsevier.com/locate/apcatb

Gold nanoparticles on titanium oxide effective for photocatalytic hydrogen formation under visible light

Hayato Yuzawa [a], Tomoko Yoshida [b], Hisao Yoshida [a,*]

[a] Department of Applied Chemistry, Graduate School of Engineering, Nagoya University, Nagoya, 464-8603, Japan
[b] Division of Integrated Research Project, EcoTopia Science Institute, Nagoya University, Nagoya, 464-8603, Japan

ARTICLE INFO

Article history:
Received 31 October 2011
Received in revised form
14 December 2011
Accepted 16 December 2011
Available online 28 December 2011

Keywords:
Plasmonic photocatalysis
Visible light
Hydrogen formation
Au nanoparticles
Titanium oxide

ABSTRACT

Photocatalytic hydrogen production from aqueous ethanol was investigated over Au-loaded titanium oxide under visible light (510–740 nm) irradiation. Hydrogen was constantly produced through the present plasmonic photocatalysis. In this system, Au nanoparticles with larger particle size were essentially effective for the reaction due to the high efficiency for the localized surface plasmon resonance (LSPR). Further, Au nanoparticles with short rod-like shapes were more effective for the reaction than those with spherical shape because of the higher efficiency for the electron transfer from the Au nanoparticle to the conduction band of titanium oxide. On the other hand, aggregates of the Au nanoparticles were not appropriate for the reaction, which derived from the low efficiency of the electron transfer. Finally, titanium oxide containing anatase phase with larger particle size was most preferred for the reaction.

1. Introduction

The solar energy conversion to hydrogen by using photocatalyst has attracted much attention [1–4]. Because of the large distribution of visible light in the solar light, new methodologies for utilization of visible light have been still required for further development of the photocatalytic technology.

Recently, localized surface plasmon resonance (LSPR) on metal nanoparticles has been applied to the visible light photocatalysis. Nowadays, alternative mechanisms for the plasmonic photocatalyses are known: one is that the LSPR in metal nanoparticles, such as Ag [5,6] and Au [7–9] nanoparticles, under visible light can enhance the local electric field of the neighboring semiconductors, such as TiO_2 [5–8] and CdS [9], to increase the original photocatalytic activities of the semiconductors. Another is that the electrons in the metal nanoparticles, such as Au [10–18], Ag [19] and Pt nanoparticles [20], can be excited by the LSPR with the visible light absorption and partly transferred to the conduction band of the attached semiconductors such as TiO_2, and the separated electrons and holes can contribute to the reductive and oxidative reactions, respectively, as shown in Fig. 1 [10,11].

The plasmonic photocatalysis for hydrogen production has also been investigated according to each mechanism. For example, for both mechanisms the observation of photocurrent promised hydrogen production [8,17]. Chen et al. reported that the electric field derived from the LSPR of Au nanoparticles enhanced water splitting over a TiO_2 photocatalyst [7]. Torimoto et al. demonstrated that dehydrogenation of propanol on a Rh/CdS photocatalyst was enhanced by the LSPR of Au nanoparticles [9]. Silva et al. reported that Au nanoparticles on TiO_2 promoted hydrogen production via electron transfer from aqueous solutions of EDTA or methanol [18]. So far, although the Au/TiO_2 plasmonic photocatalysts have been often studied by many researchers for many reactions, key factors of the Au/TiO_2 plasmonic photocatalysts effective for the hydrogen production have not been investigated in detail.

In the present study, we studied the plasmonic photocatalysis with the electron transfer on the Au/TiO_2 system for hydrogen evolution from an aqueous ethanol. We prepared various Au-loaded titanium oxide samples and examined the reaction test by using strictly limited visible light (510–740 nm in wavelength) in order to rule out the contribution of the original photocatalytic activity of the TiO_2 which can be excited with UV light. As a result, we clarified the effective Au nanoparticles for the present hydrogen formation system according to the electron transfer mechanism.

* Corresponding author. Tel.: +81 52 789 4609; fax: +81 52 789 3178.
E-mail address: yoshidah@apchem.nagoya-u.ac.jp (H. Yoshida).

0926-3373/$ – see front matter © 2011 Elsevier B.V. All rights reserved.
doi:10.1016/j.apcatb.2011.12.029

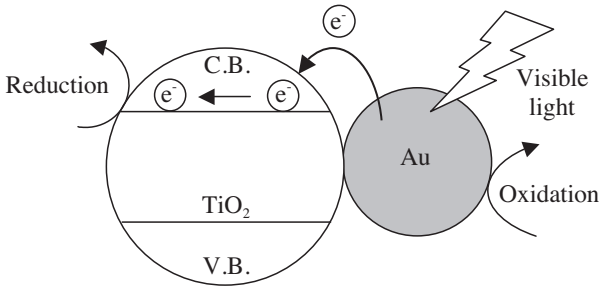

Fig. 1. Proposed mechanism for the plasmonic photocatalysis on Au-loaded titanium oxide from ref. [10,11].

2. Experimental

2.1. Reagents

Titanium oxide samples, JRC-TIO-8 (anatase, 338 $m^2 g^{-1}$), JRC-TIO-6 (rutile, 100 $m^2 g^{-1}$), JRC-TIO-4 (anatase/rutile, 50 ± 15 $m^2 g^{-1}$) and JRC-TIO-5 (rutile 2.7 $m^2 g^{-1}$) were supplied by Catalysis Society of Japan and they were referred to as TIO-A300, TIO-R100, TIO-AR50 and TIO-R3, respectively in this paper. Precursor of Au nanoparticles was gold chloride acid tetrahydrate ($HAuCl_4 \cdot 4H_2O$, Kishida, 99%). Other reagents were methanol (Kishida, 99.8%), ethanol (Kishida, 99.5%), citric acid (Kishida, 99.5%) and aqueous sodium hydroxide solution (Wako, 30%, w/v). These reagents were used as received.

2.2. Preparation and characterization of the Au-loaded titanium oxide

Various Au-loaded titanium oxide samples were prepared by two methods; a conventional photodeposition method and a nanoparticles photodeposition method. In the former method, the titanium oxide powder (4 g) was dispersed into an aqueous methanol solution (400 ml, methanol concentration 25%) of the Au precursor in a beaker with vigorous stirring, followed by photoirradiation from the top with a 300 W Xe lamp, which emitted both UV and visible light, in atmospheric condition for 3 h. Then, the suspension was filtered off with suction, washed with water, and dried at 323 K overnight. The loading amount was 0.1, 0.5, 1.0 and 2.0 wt% for each titanium oxide sample, and additionally 3.0 and 4.0 wt% for the TIO-R3 sample. In this paper, *x* wt% Au-loaded titanium oxide prepared in this photodeposition method is described as $Au(x)_p/TiO_2$.

In the latter method, a stock solution of Au nanoparticles was prepared by a citrate reduction method [21,22]. Both a mixture of an aqueous citric acid solution (0.39 g/11 ml) and 30%(w/v) sodium hydroxide solution (0.75 ml) and another aqueous solution (250 ml) containing $HAuCl_4 \cdot 4H_2O$ (83.6 mg) were heated to 353 K, and the former solution was added to the latter solution with stirring. The mixture was maintained at the temperature with stirring for 30 min to reduce Au(III) completely and then cooled down to room temperature to obtain the stock solution of Au nanoparticles. The TIO-A300 (2 g) sample was dispersed into the objective amount of the stock solution diluted to 270 ml by distilled water in a quartz beaker with vigorous stirring, followed by photoirradiation from the side with the 300 W Xe lamp in air atmosphere for 24 h. The suspension was filtered off with suction, washed with water, and dried at 323 K overnight. To examine the influence of the specific surface area of the titanium oxide, TIO-A50 (anatase, 50 $m^2 g^{-1}$) was prepared by calcination of the TIO-A300 sample at 873 K for 24 h. Then, 0.1 wt% Au-loaded TIO-R100, TIO-AR50 and TIO-A50 samples were also prepared by the same procedure. For the TIO-R3 sample, after the photoirradiation, the solvent was evaporated from the similarly obtained suspension at 333 K in 1.2×10^4 Pa to dryness. The obtained sample was again dispersed into water (80 ml) and recovered by centrifugation, which was done three times. The sample was dried at 323 K overnight and further photoirradiated by the 300 W Xe lamp for 48 h in air atmosphere. In this paper, *x* wt% Au-loaded titanium oxide prepared in this method is described as $Au(x)_{np}/TiO_2$.

Diffuse reflectance UV–vis spectra of the prepared $Au(x)/TiO_2$ samples were recorded with a JASCO V-570 spectrophotometer. TEM image was observed with a JEOL electron microscope (JEM-2100M, 200 kV) equipped with a CCD camera (Gatan, erlangshen ES 500W).

2.3. Photocatalytic reaction test

Photocatalytic hydrogen production from aqueous ethanol was examined in a closed reactor connected with a vacuum line. The prepared $Au(x)/TiO_2$ (0.5 g) sample in a quartz cell was photoirradiated from beneath (18 cm^2) by the Xe lamp with atmospheric oxygen for 1 h to clean up the catalyst surface. The air in the reactor was evacuated for 10 min and Ar (9.9×10^4 Pa) was introduced. After ethanol (2 ml, corresponding to 34 mmol) and water (2 ml, corresponding to 56 mmol) were introduced, the photocatalyst was photoirradiated with stirring for 24 h by another 300 W Xe lamp (Asahi spectra, MAX-302) equipped with both a mirror module permitting the light of 385–740 nm in wavelength and an optical cut-off filter permitting the light of longer than 510 nm in wavelength. This Xe lamp emits the visible light only (510–740 nm in wavelength) with similar intensity for each wavelength. The transmittance spectrum of the cut-off filter is shown in Fig. 2a. The wavelength of the absorption edge for the bandgap excitation of each titanium oxide sample was sufficiently shorter than the wavelength range of the irradiated light (510–740 nm) in the present photocatalytic reaction test as shown in Fig. 2a. Thus, the bandgap excitation of the titanium oxide can be ruled out during the photocatalytic reaction test in the present study. Gas products were collected by a gas tight syringe and analyzed by a GC-TCD (Shimadzu, GC-8A). The objective reaction was ethanol oxidation to yield hydrogen and oxidation products such as acetaldehyde and carbon dioxide, which is a well-known photocatalysis over metal loaded titanium oxide under irradiation of UV light [23]. In this system, the partial oxidation from ethanol to aldehyde (Eq. (1)) mainly occurs at the early stage with low conversion. In the present study, the reaction test was performed at low conversion level (less than 0.05% for 24 h), the main reaction can be described as shown in Eq. (1).

$$C_2H_5OH \xrightarrow[Au/TiO_2]{h\nu} CH_3CHO + H_2 \quad (1)$$

Only when the reaction was carried out for 24 h, we sometimes detected very small amount of carbon dioxide, meaning that the complete oxidation also occurred minor at such time. Apparent quantum efficiency was calculated as following equation.

$$\text{Apparent quantum efficiency (\%)} = 100 \times \frac{2 \times (\text{hydrogen yield [mol]})}{(\text{incident photons from 510 to 740 nm [mol]})} \quad (2)$$

3. Results and discussion

3.1. Characterization of the prepared Au-loaded TiO_2 samples

Fig. 2 shows DR UV–vis spectra of the TiO_2 supports and the $Au(x)_p/TiO_2$ samples with TEM images of the $Au(2.0)_p/TiO_2$ samples. In all of the $Au(x)_p/TiO_2$ samples, the absorption band

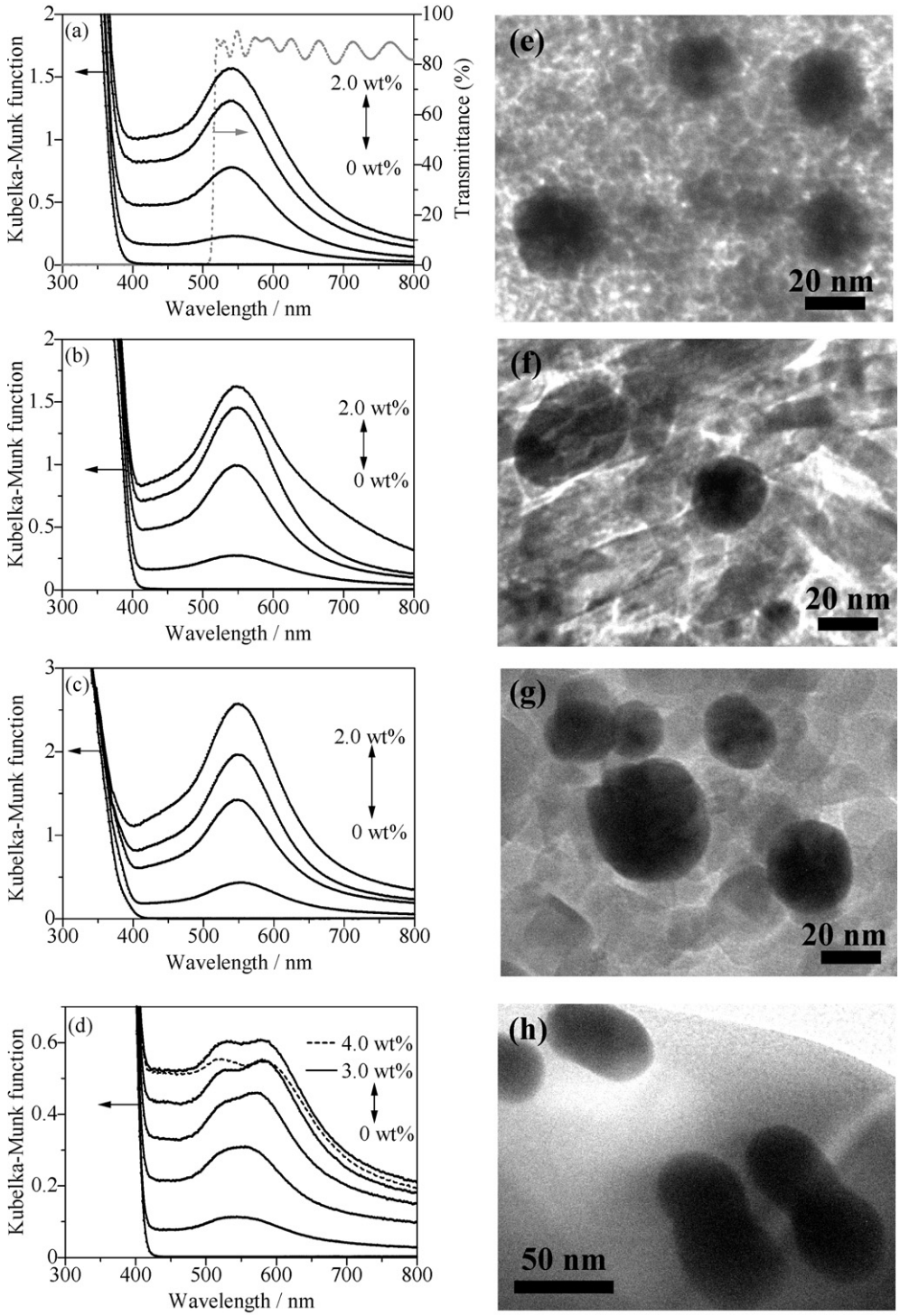

Fig. 2. DR UV–vis spectra of the Au(x)$_p$/TiO$_2$ (x = 0, 0.1, 0.5, 1.0 and 2.0 wt%) samples with TIO-A300 (a), TIO-R100 (b) and TIO-AR50 (c), and the Au(x)$_p$/TIO-R3 (x = 0, 0.1, 0.5, 1.0, 2.0, 3.0 and 4.0 wt%) sample (d), which were prepared with the conventional photodeposition method, and TEM images of the samples: Au(2.0)$_p$/TIO-A300 (e), Au(2.0)$_p$/TIO-R100 (f), Au(2.0)$_p$/TIO-AR50 (g) and Au(2.0)$_p$/TIO-R3 (h). Dotted line in (a) is a transmission spectrum of the optical cut-off filter (λ > 510 nm) used in the photocatalytic reaction.

assignable to the LSPR on Au nanoparticles was observed around 550 nm besides the bandgap absorption (<400 nm) of each titanium oxide, confirming the existence of Au nanoparticles in the samples. The wavelength at the maximum of the LSPR band (λ_{max}) was slightly different from each other, and the absorption intensity was also considerably different from sample to sample. The intensity of the LSPR band increased with increasing Au loading amount, except for the Au(4.0)$_p$/TIO-R3 sample. These would be because the λ_{max} and the absorption intensity depended on the size, the shape and the environment of the Au nanoparticles [24]. In the Au(x)$_p$/TIO-A300, Au(x)$_p$/TIO-A100 and Au(x)$_p$/TIO-AR50 samples (Fig. 2a–c), the shape of the LSPR band was similar, indicating that the size, shape and the environment of Au nanoparticles were similar to each other. This was supported by the TEM images of each

$Au(2.0)_p/TiO_2$ sample, where almost spherical nanoparticles were observed (Fig. 2e–g).

On the other hand, in the spectra of the $Au(x)_p$/TIO-R3 samples (Fig. 2d), although one absorption peak (λ_{max} = 543 nm) was observed for the $Au(0.1)_p$/TIO-R3 sample, the band gradually split into two bands with increasing the Au loading amount, indicating that rod-like Au nanoparticles [14,25,26] formed in the $Au(x)_p$/TIO-R3 sample with higher loading amount. In fact, in addition to the spherical nanoparticles, the rod-like nanoparticles were also observed for the $Au(2.0)_p$/TIO-R3 (Fig. 2h). As for the rod-like nanoparticles on the sample, the length for the long axis was distributed from 52 to 132 nm, that for the short axis was from 24 to 52 nm, and the aspect ratio was distributed from 1.7 to 3.0.

Table 1 summarizes the average Au nanoparticles size (D_{Au}) calculated from the values of more than 100 particles observed by the TEM for each sample, and the number density of the Au nanoparticles (N_{Au}) calculated from the D_{Au} value and the density of Au metal (19.32 g/cm^3) under the assumption that all the Au nanoparticles were spherical. As for the $Au(2.0)_p$/TIO-R3 and $Au(4.0)_p$/TIO-R3 samples (Table 1, entries 6 and 7), the average for both the spherical particles and the rod-like particles (with long and short axes) are listed together. For these samples, the N_{Au} value could not be correctly calculated since the shape distribution of the Au nanoparticles (spherical and rod-like) could not be accurately estimated from the TEM observation. However, by using the average diameter of the spherical particles, we can estimate the N_{Au} values to be less than 5.1×10^{13} and 3.2×10^{13} $(g\,TiO_2)^{-1}$ for the $Au(2.0)_p/TiO_2$ and $Au(4.0)_p/TiO_2$ samples, respectively.

Among the $Au(2.0)_p/TiO_2$ samples, the average size of the Au nanoparticles increased with decreasing the specific surface area of the titanium oxide (Table 1, entries 1, 2, 4 and 6). This might be because the Au nanoparticles would grow more easily on the titanium oxide surface of low specific surface area under photoirradiation, or the relatively small number of defects on the large titanium oxide particles would induce a small number of Au nuclei generation to produce large particles as proposed in literature [14].

The average Au nanoparticles size in the $Au(0.5)_p$/TIO-AR50 sample was 11.3 nm (Table 1, entry 3), which was smaller than that in the $Au(2.0)_p$/TIO-AR50 sample (25.3 nm, Table 1, entry 4). On the other hand, the number density of Au nanoparticles (N_{Au}) for the $Au(0.5)_p$/TIO-AR50 sample was larger than that for the $Au(2.0)_p$/TIO-AR50 sample, which were 3.4×10^{14} and 1.2×10^{14} $(g\,TiO_2)^{-1}$, respectively (Table 1, entries 3 and 4). Further, among the samples with the TIO-R3 support (Table 1, entries 5–7), the same tendency was observed, confirming that the average size of the Au nanoparticles increased and the number density of the Au nanoparticles decreased with increasing the Au loading amount. These suggest that the growth and aggregation of the Au nanoparticles occurred more easily than nucleation of the Au nanoparticles when the larger amount of Au was loaded on the titanium oxide surface in the present photodeposition method.

Fig. 3a and d shows the UV–vis absorption spectrum of the Au nanoparticle colloid solution prepared by the citrate reduction method (the stock solution) and the TEM image of the extracted Au nanoparticles from the solution. The shape of the LSPR band in the spectrum was sharp (Fig. 3a), suggesting that Au nanoparticles with narrow size distribution were formed in the solution. Further, the TEM image (Fig. 3d) shows almost uniform spherical Au nanoparticles with narrow size distribution from 11 to 15 nm in diameter (average particle size: 12.8 nm, Table 1, entry 8). These results confirmed that the spherical Au nanoparticles stabilized with the citric acid were obtained with the narrow size distribution as reported in literature [22]. These nanoparticles were loaded on the TIO-A300 and TIO-R3 supports with photoirradiation. In the $Au(x)_{np}$/TIO-A300 samples, the shape of the LSPR band in the DR UV–vis spectra was similar to that of the Au nanoparticle colloid solution (Fig. 3b). Further, the TEM image of the $Au(2.0)_{np}$/TIO-A300 sample shows Au nanoparticles having the narrow size distribution (average particle size: 14.6 nm) similar to those in the solution (Fig. 3e and Table 1, entry 9). This indicates that the Au nanoparticles were by the citrate reduction method would be loaded on the TIO-A300 surface almost as they were. Thus, it is deduced that the number density of the Au nanoparticles on the TIO-A300 should increase with increasing the loading amount until at least 2.0 wt%. On the other hand, in the $Au(x)_{np}$/TIO-R3 samples, the shape of the LSPR band considerably became broad with an increase of the Au loading amount although the sharp absorption band was observed only for the $Au(0.1)_{np}$/TIO-R3 sample (Fig. 3c). The TEM images of the $Au(2.0)_{np}$/TIO-R3 sample revealed that the loaded Au nanoparticles gathered together (Fig. 3f), the size of the Au nanoparticles became larger, some of them were more large (ca. 30–50 nm), and thus the average particle size increased to some extent (17.8 nm, Table 1, entry 10). These suggest that the aggregates and the large nanoparticles would absorb the light of longer wavelength, as reported in literature [24].

3.2. Outline of the photocatalytic reaction

Table 2 shows the results of the photocatalytic reaction tests for the $Au(0.1)_p$/TIO-A300 sample as representative. When the photocatalytic reaction test was carried out, hydrogen production (10.5 μmol) was observed (Table 2, entry 1). The control tests were also carried out without the loading of Au nanoparticles (entry 2), without the photocatalyst (entry 3) and without the photoirradiation (entry 4). In these cases, no hydrogen was observed, confirming that the photoexcitation of the Au nanoparticles with the visible light (510–740 nm), which would correspond to the LSPR or inter/intra band excitation [12], should play an important role for the hydrogen generation. For all the other $Au(x)_p/TiO_2$ samples and the $Au(x)_{np}/TiO_2$ samples, the same conclusion was obtained.

Fig. 4 shows time courses of the hydrogen yield over two representatives, i.e., the $Au(0.1)_p$/TIO-A300 sample and the $Au(0.1)_p$/TIO-R3 sample. These samples, as well as all other samples in the present study, promoted hydrogen production almost constantly at least 24 h. To exclude the possibility of the stoichiometric chemical reaction, the turn over number (TON) was calculated: the amount of the produced hydrogen for 24 h over the $Au(0.1)_p$/TIO-A300 sample was divided by the number of the Au atoms in the sample. The value was 10.3, which exceeded the unity. These support that the hydrogen evolution proceeded photocatalytically.

As representatively shown in Fig. 4a, some samples exhibited each short induction period. The induction period was more clearly observed for the samples with the larger specific surface area of the titanium oxide. To elucidate this phenomenon, the recycle uses were examined as shown in Fig. 4a. After the first run with the fresh sample, the gas phase was purged by Ar and the second run started. In this case, the induction period was not observed (Fig. 4a, open circle). On the other hand, when the second reaction was carried out after the product gas was purged by O_2 and then purged by Ar, the induction period was again observed. These results indicate that the titanium oxide surface was once reduced by the produced hydrogen, or by the photoexcited electron transferred from the Au nanoparticles, at the initial stage of the reaction. When purged by O_2, the surface would be reoxidized by O_2. Thus, it is suggested that the initial reduction of the titanium oxide surface was required before the successive stable production of hydrogen. However, it is difficult to determine whether the surface reduced sites were necessary for the photocatalytic reaction, or not, at present.

Among the investigated samples the highest apparent quantum efficiency was 0.26% in the present reaction condition under the

Table 1
Various properties for the Au-loaded TiO_2 samples.

Entry	Sample	D_{Au}[a] (nm)	N_{Au}[b]/10^{14} ($g\,TiO_2$)$^{-1}$	Y_{H_2} (μmol)[c]	I_{LSPR}/N_{Au}[d] (10^{-14})	Y_{H_2}/I_{LSPR}	Y_{H_2}/N_{Au} (10^{-19} mol)
1	$Au(2.0)_p$/TIO-A300	18.6	3.1	7.2	1.7	6.9	1.2
2	$Au(2.0)_p$/TIO-R100	21.9	1.9	5.0	2.9	4.6	1.3
3	$Au(0.5)_p$/TIO-AR50	11.3	3.4	17.5	1.4	19	2.6
4	$Au(2.0)_p$/TIO-AR50	25.3	1.2	12.3	6.9	7.2	5.0
5	$Au(0.5)_p$/TIO-R3	13.4	2.1	13.5	0.50	65	3.3
6	$Au(2.0)_p$/TIO-R3	33.7[e] 81.4/36.7[g]	<0.51[f]	19.2	>3.3[f]	55	>19[f]
7	$Au(4.0)_p$/TIO-R3	49.8[e] 110.1/49.9[g]	<0.32[f]	20.2	>5.7[f]	56	>31[f]
8	Au colloid	12.8	9.4[h]	–	–	–	–
9	$Au(2.0)_{np}$/TIO-A300	14.6	6.4	3.6	0.79	3.6	0.28
10	$Au(2.0)_{np}$/TIO-R3	17.8	3.5	0.5	0.8	0.89	0.071

[a] D_{Au} = the average size of the Au nanoparticles. This was calculated from the values more than 100 particles observed by the TEM.
[b] N_{Au} = the number density of the Au nanoparticles. This value was calculated from the D_{Au} value and the density of Au metal, 19.32 g/cm^3.
[c] Y_{H_2} = the hydrogen yield in the photocatalytic reaction test. Catalyst: 0.5 g, aqueous ethanol solution (50%): 4 ml, irradiated light intensity: 10 mW/cm^2 in the range of 510–740 nm, and reaction time: 24 h.
[d] I_{LSPR} = the LSPR intensity at λ_{max} in the DR UV–vis spectrum (Kubelka-Munk function).
[e] The average size of the spherical Au nanoparticles.
[f] Calculated by using the D_{Au} value of the spherical Au nanoparticles.
[g] The average size of the short rod-like Au nanoparticles (with the long/short axes).
[h] Calculated as the quantity equivalent to the 2.0 wt% Au loading.

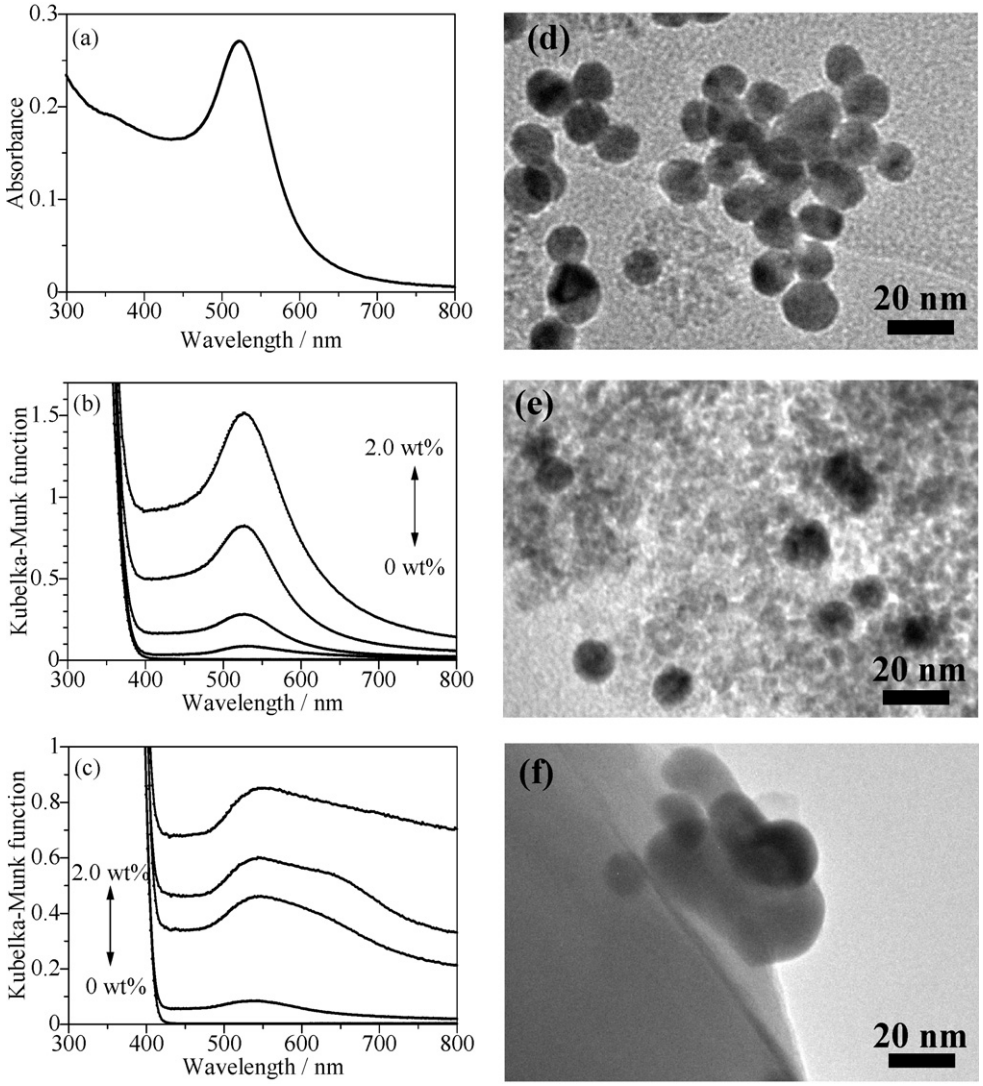

Fig. 3. UV–vis absorption spectrum of the Au nanoparticles colloid solution prepared with the citrate reduction method (a) and DR UV–vis spectra of the $Au(x)_{np}/TiO_2$ (x = 0, 0.1, 0.5, 1.0 and 2.0 wt%) samples with TIO-A300 (b) and TIO-R3 (c) prepared by the nanoparticles photodeposition method, and TEM images of the extracted Au nanoparticles from the solution (d), the $Au(2.0)_{np}$/TIO-A300 (e) and $Au(2.0)_{np}$/TIO-R3 (f) samples.

Table 2
Results of the photocatalytic reaction tests.[a]

Entry	Sample	Irradiated light wavelength (nm)	H_2 yield (μmol)
1	$Au(0.1)_p$/TIO-A300	510–740	10.5
2	TIO-A300	510–740	n.d.[b]
3[c]	–	510–740	n.d.[b]
4[d]	$Au(0.1)_p$/TIO-A300	–	n.d.[b]

[a] Catalyst: 0.5 g, aqueous solution of ethanol (50%): 4 ml, irradiated light intensity: 10 mW/cm^2 in the range of 510–740 nm, reaction time: 24 h. Detection limit for hydrogen was 0.02 μmol.
[b] n.d. = not detected.
[c] Photochemical reaction without the photocatalyst.
[d] Reaction at room temperature without photoirradiation.

light of 510–740 nm in wavelength, which was recorded over the $Au(0.1)_p$/TIO-AR50 and $Au(4.0)_p$/TIO-R3 samples.

3.3. Influence of the Au loading amount

Fig. 5 shows the hydrogen yield over the prepared samples. In the case of the samples with the TIO-A300, R100 and AR50 supports, the hydrogen yield decreased with increasing the Au loading amount (Fig. 5a–c). This tendency was opposite to the absorption intensity of the Au nanoparticles, indicating that the photoexcited electrons in the Au nanoparticles would not be efficiently used for the hydrogen production on the samples of the high Au loading. The obtained tendency of the hydrogen yield for the above samples would be derived from the increase of the Au nanoparticles size, and the decrease of the number density of the Au nanoparticles. On the other hand, as for the $Au(x)_p$/TIO-R3 samples, the hydrogen yield increased with increasing the Au loading amount (Fig. 5d), which was similar to the variation of the photoabsorption intensity except for the $Au(0.5)_p$/TIO-R3 sample. As mentioned above, in contrast to the other $Au(x)_p/TiO_2$ samples, the $Au(x)_p$/TIO-R3 samples contained the short rod-like Au nanoparticles. Thus, two possibilities can be suggested: the short rod-like Au nanoparticles might be more effective for the reaction than the spherical Au nanoparticles or the property of this TIO-R3 might be different from the other titanium oxides.

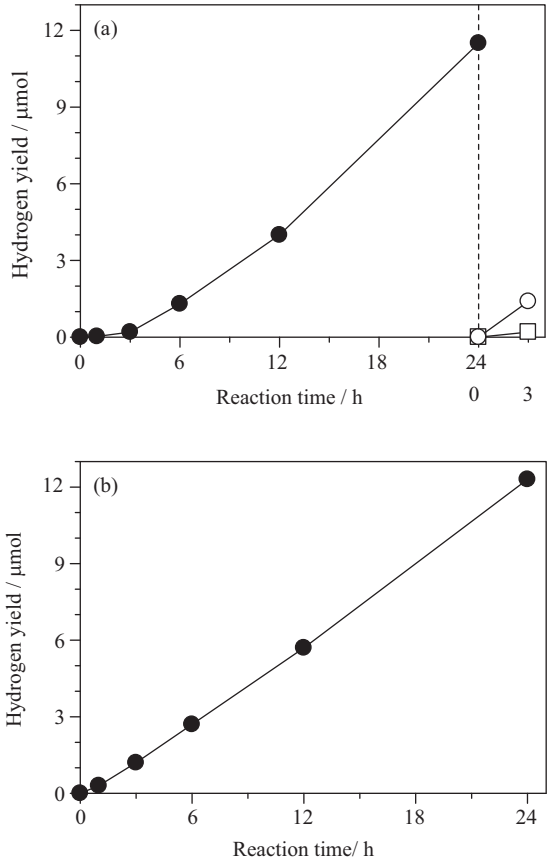

Fig. 4. Time course of the hydrogen yield over the $Au(0.1)_p$/TIO-A300 sample (a) and the $Au(0.1)_p$/TIO-R3 sample (b). Open circle shows the results of the recycle tests over the $Au(0.1)_p$/TIO-A300 sample after the gas phase was purged by Ar. Open square shows the result of the recycle reaction after the product gas was purged by O_2 and then purged by Ar. As for the reaction condition, see the footnote a of Table 2.

Fig. 5e and f shows the result of the hydrogen yield over the $Au(x)_{np}$/TIO-A300 and $Au(x)_{np}$/TIO-R3 samples. On the $Au(x)_{np}$/TIO-A300 samples, hydrogen yield decreased with increasing Au loading amount. The shape and size of Au nanoparticles were almost uniform in these samples and the number of the nanoparticle linearly increased with an increase of the loading amount as evidenced by the almost linear increase of the photoabsorption intensity. These results suggest that the increase of the number density of the Au nanoparticles would provide negative effect on the photocatalytic activity. Over the $Au(x)_{np}$/TIO-R3 samples, the hydrogen yield decreased more rapidly than that over the $Au(x)_{np}$/TIO-A300 samples with increasing the Au loading amount. Thus, it is suggested that the aggregates of the Au nanoparticles as shown in Fig. 3f would have less ability to produce for the hydrogen.

3.4. Au nanoparticles effective for the hydrogen production

To compare the efficiency of each reaction step in the plasmonic photocatalysis in detail among the samples, Table 1 summarizes the LSPR intensity at λ_{max} per single Au nanoparticle (I_{LSPR}/N_{Au}), the ratio of the hydrogen yield to the LSPR intensity at λ_{max} (Y_{H_2}/I_{LSPR}) and the hydrogen yield per single Au nanoparticle (Y_{H_2}/N_{Au}). The I_{LSPR}/N_{Au} values would reflect the photoexcitaion efficiency of the Au nanoparticles, and the Y_{H_2}/I_{LSPR} value would show the total efficiency of the electron transfer from the Au nanoparticles to the conduction band of titanium oxide and the successive hydrogen production. As we know, in the case of powder sample, the absolute evaluation of absorption intensity in LSPR is impossible because the diffusion of the light cannot be ignored. Thus, Kubelka–Munk function is usually employed to estimate the absorbance as a better approximation, although even using it the complete estimation is impossible for lack of the correct scattering coefficient. In the present study, we adopted the intensity at λ_{max}, I_{LSPR}, which is obtained through Kubelka–Munk function, as the approximate value for the absorption to discuss the relative relationship among the samples. Although we also examined to use the reflectance to estimate the absorption without considering the diffusion, we obtained the same relationships as the present ones.

Among the $Au(x)_p$/TIO-AR50 samples (Table 1, entries 3 and 4), with increasing the Au loading amount, the LSPR intensity at λ_{max} per single Au nanoparticle (I_{LSPR}/N_{Au}) increased but the ratio of hydrogen yield to LSPR intensity at λ_{max} (Y_{H_2}/I_{LSPR}) decreased. Thus, the spherical Au nanoparticles having larger particle size

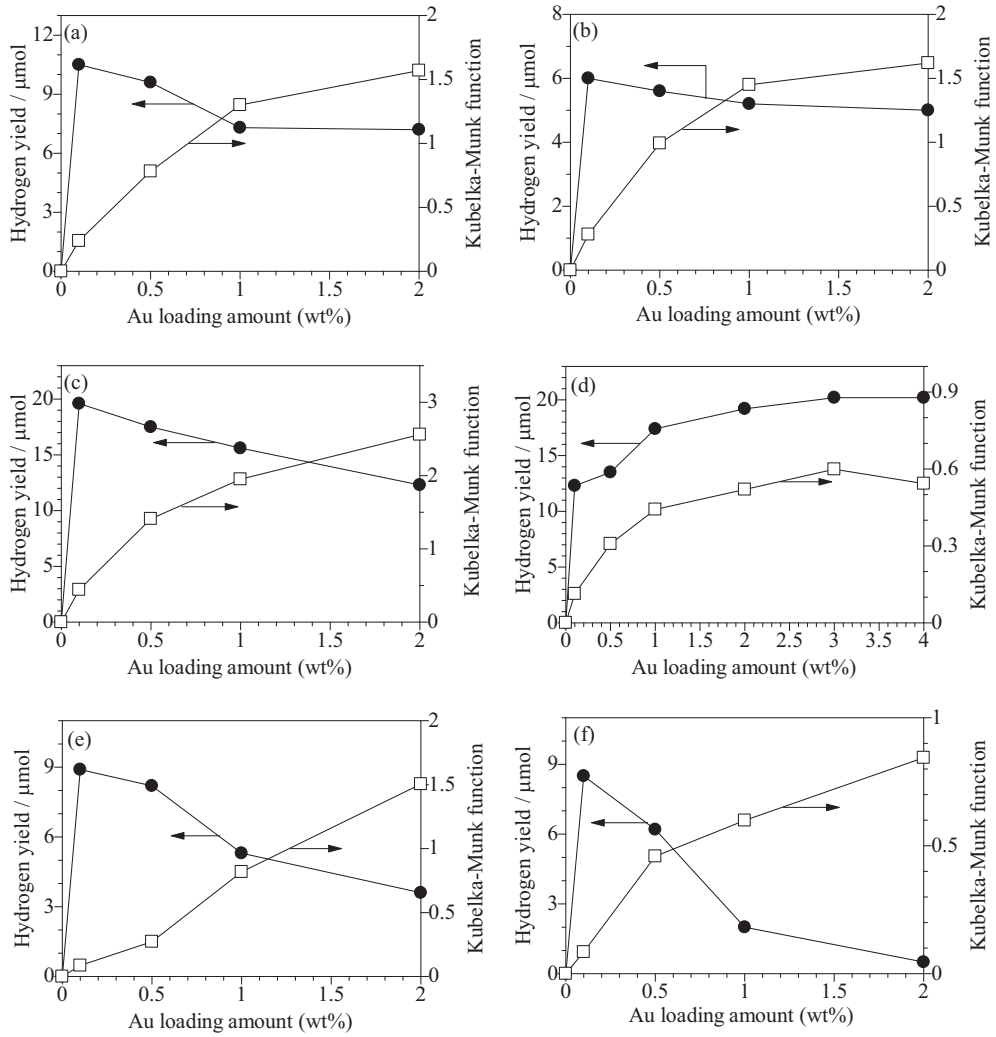

Fig. 5. Hydrogen yield over the samples and the absorption intensity of the LSPR band at λ_{max} for the samples: the Au(x)$_p$/TIO-A300 samples (a), the Au(x)$_p$/TIO-R100 samples (b), the Au(x)$_p$/TIO-AR50 samples (c), the Au(x)$_p$/TIO-R3 samples (d), the Au(x)$_{np}$/TIO-A300 samples (e) and the Au(x)$_{np}$/TIO-R3 samples (f). As for the reaction condition, see the footnote a of Table 2.

would be more effective for the hydrogen production because of the higher photoabsorption efficiency, despite the lower efficiency for the electron transfer to the titanium oxide.

Among the Au(x)$_p$/TIO-R3 samples (Table 1, entries 5–7), the I_{LSPR}/N_{Au} value increased with increasing the Au loading amount similarly to the Au(x)$_p$/TIO-AR50 samples. However, the Y_{H_2}/I_{LSPR} value did not vary with an increase of the Au loading amount in contrast to the Au(x)$_p$/TIO-AR50 samples. As a result, among the Au(2.0)$_p$/TiO_2 samples, the highest Y_{H_2}/N_{Au} value was observed for the Au(2.0)$_p$/TIO-R3 sample. The Au(4.0)$_p$/TIO-R3 sample exhibited the highest Y_{H_2}/N_{Au} value in the samples listed in Table 2. Thus, compared to the spherical Au nanoparticles, the short rod-like Au nanoparticles should be more effective for the reaction. This would be because the short rod-like Au nanoparticles provided higher efficiency for the electron transfer to the titanium oxide than the spherical Au nanoparticles. In the samples containing the short rod-like Au nanoparticles, i.e., the Au(2.0)/TIO-R3 and Au(4.0)/TIO-R3 samples, the latter exhibited the higher Y_{H_2}/N_{Au} and I_{LSPR}/N_{Au} values than the former (Table 1, entries 6 and 7). This implies that the larger size of the short rod-like Au nanoparticles might contribute to the high efficiency for the LSPR and thus more efficient for the reaction. However, at present there is no clear evidence to clarify it because both the distribution and the size of the rod-like Au nanoparticles might simultaneously vary with the Au loading amount. If the above-mentioned tendency for the spherical Au nanoparticles could be applied to this case, it is expected that the rod-like Au nanoparticles with larger particles size would be more effective for the reaction.

In the Au(2.0)$_{np}$/TIO-R3 sample (Table 1, entry 10), the Y_{H_2}/N_{Au} value was the lowest among all of the samples, which would be due to the lowest Y_{H_2}/I_{LSPR} value. This suggests that the aggregates (Fig. 3f) in this sample would not be appropriate for the reaction because of the low efficiency of the electron transfer.

In the Au(2.0)$_{np}$/TIO-A300 sample (Table 1, entry 9), the Y_{H_2}/N_{Au} value was lower compared to the samples with the similar size of the Au particles, such as the Au(0.5)$_p$/TIO-AR50 and Au(0.5)$_p$/TIO-R3 samples (Table 1, entries 3 and 5). The hydrogen yield shown in Fig. 5e decreased with increasing the Au loading amount, although the number of the Au nanoparticles increased and no aggregates was observed on the TEM images (Fig. 3e). These results suggest that the sufficient interaction between the Au nanoparticles and the titanium oxide would not be attained because of the incomplete removal of the citrate ligand for the samples of high Au content, and as a result, the number of the practically active Au nanoparticles would decrease with increasing loading amount. Thus, further improvement of the nanoparticles photodeposition method is desired to obtain the samples of high content. On the other hand, in the case of the Au(0.1)$_{np}$/TIO-A300 sample, it seems

Table 3
Results of the photocatalytic reaction tests over $Au(0.1)_{np}/TiO_2$ samples.[a]

Entry	Sample	H_2 yield (μmol)
1	$Au(0.1)_{np}$/TIO-A50	20.7
2	$Au(0.1)_{np}$/TIO-AR50	19.5
3	$Au(0.1)_{np}$/TIO-A300	8.9
4	$Au(0.1)_{np}$/TIO-R3	8.5
5	$Au(0.1)_{np}$/TIO-R100	5.0

[a] As for the reaction condition, see the footnote a of Table 2.

that the Au nanoparticles were effective for the hydrogen production. The hydrogen yield on the $Au(0.1)_{np}$/TIO-A300 sample was similar to that for the $Au(0.1)_p$/TIO-A300 (Fig. 5a and e). This fact suggests that the Au nanoparticles prepared by the citrate reduction method is loaded on the titanium oxide with the sufficient interaction on the samples, and the both preparation methods in the present study would be similarly usable at least for the samples of low Au content.

Thus, it was revealed that the photocatalytic activity was influenced by various factors of the Au nanoparticles such as the size, the shape, and the dispersibility: the large particle size of the Au nanoparticles (at least the spherical ones) would be effective for this reaction because of the high LSPR efficiency, and the short rod-like shape would be effective for this reaction because of the high efficiency for the electron transfer from the Au nanoparticles to the TiO_2 support. The aggregates of the Au nanoparticles would be unfavorable due to the low efficiency of the electron transfer.

3.5. Titanium oxide effective for the hydrogen production

The effect of the titanium oxide on the activity in the present plasmonic photocatalysis will be discussed here. For this purpose, the samples of the low Au loading amount prepared with the nanoparticles photodeposition method, i.e., the $Au(0.1)_{np}/TiO_2$ samples, would be appropriate because they would have the low number density and the uniform size and shape of the Au nanoparticles. Table 3 shows the hydrogen yield for each sample. As a result, the order of the hydrogen yield was $Au(0.1)_{np}$/TIO-A50 ≈ $Au(0.1)_{np}$/TIO-AR50 > $Au(0.1)_{np}$/TIO-A300 ≈ $Au(0.1)_{np}$/TIO-R3 > $Au(0.1)_{np}$/TIO-R100 (Table 3, entries 1–4). This tendency indicates that the samples with anatase exhibited the higher photocatalytic activity than the samples with rutile. It would be because anatase has the higher energy level of conduction band (−0.20 V vs NHE) than that of rutile (+0.04 V) and the electrons in the conduction band would more easily contribute to the reductive reaction as reported in literature for various photocatalytic reactions under UV light irradiation [27,28].

Fig. 6 summarizes the relationship between the hydrogen yield over the $Au(0.1)_{np}/TiO_2$ samples and the specific surface area of these titanium oxides. Among the samples with anatase, the two samples with the lower specific surface area (the $Au(0.1)_{np}$/TIO-A50 and $Au(0.1)_{np}$/TIO-AR50 samples) exhibited higher activity than the $Au(0.1)_{np}$/TIO-A300 sample with high specific surface area. Also in the samples with rutile, the same tendency was observed. Thus, these results indicate that the large particle size of the titanium oxide would be effective for the hydrogen production in the present plasmonic photocatalysis. This would be because the electrons in the conduction band of the titanium oxide with the large particle size have a long life with less recombination at the defect sites as reported in literature [11,27,28].

As discussed here, the activity of the plasmonic photocatalyst, Au-loaded TiO_2, would be also influenced by the crystal phase and the size of the crystallites of the titanium oxide as often reported in the photocatalysis through the bandgap excitation of titanium oxide under UV light irradiation.

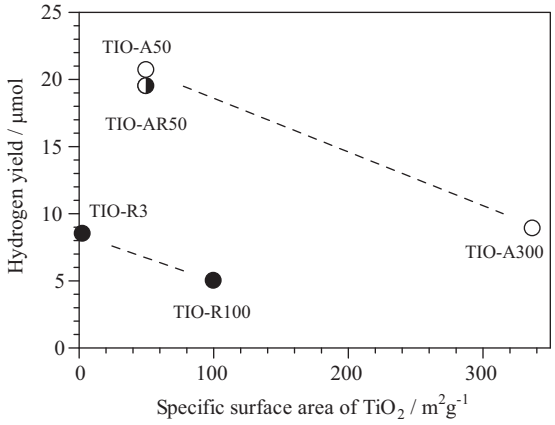

Fig. 6. The hydrogen yield over the $Au(0.1)_{np}/TiO_2$ samples with the various specific surface area of titanium oxide. Two open symbols, two filled symbols and a half filled symbol indicate anatase, rutile and anatase/rutile mixture, respectively. As for the reaction condition, see the footnote a of Table 2.

4. Conclusion

The key factors for the hydrogen production from aqueous ethanol over the Au-loaded titanium oxide induced by the LSPR of the Au nanoparticles were investigated. After the short induction period by the reduction of the titanium oxide, the reaction continuously and photocatalytically proceeded. As for the spherical Au nanoparticles on the titanium oxide, larger particle size was more effective for the reaction because of the higher efficiency of the LSPR. However, the aggregates of the Au nanoparticles were not effective for the reaction because of the low efficiency of the electron transfer to the conduction band of titanium oxide. The Au nanoparticles with the short rod-like shapes were more effective for the hydrogen production than the spherical Au nanoparticles due to the higher efficiency of the electron transfer. As for the titanium oxide, the crystal phase and the particle size were important factors for the higher photocatalytic activity, i.e., large particles of anatase were preferable.

Acknowledgements

We thank Professor S. Muto (Nagoya University) for his kindness about the TEM observation. This research was financially supported by Grant-in-Aid for Scientific Research on Priority Area "Strong Photon-Molecule Coupling Fields (no. 470)", Grant-in-Aid for JSPS fellows (22–7799) and the fund for doctoral students in Nagoya University.

References

[1] K. Maeda, K. Domen, J. Phys. Chem. C 111 (2007) 7851–7861.
[2] F.E. Osterloh, Chem. Mater. 20 (2008) 35–54.
[3] J. Zhu, M. Zäch, Curr. Opin. Colloid Int. Sci. 14 (2009) 260–269.
[4] A. Kudo, Y. Miseki, Chem. Soc. Rev. 38 (2009) 253–278.
[5] K. Awazu, M. Fujimaki, C. Rockstuhl, J. Tominaga, H. Murakami, Y. Ohki, N. Yoshida, T. Watanabe, J. Am. Chem. Soc. 130 (2008) 1676–1680.
[6] D.B. Ingram, P. Christopher, J.L. Bauer, S. Linic, ACS Catal. 1 (2011) 1441–1447.
[7] J.J. Chen, J.C.S. Wu, P.C. Wu, D.P. Tsai, J. Phys. Chem. C 115 (2011) 210–216.
[8] Z. Liu, W. Hou, P. Pavaskar, M. Aykol, S.B. Cronin, Nano Lett. 11 (2011) 1111–1116.
[9] T. Torimoto, H. Horibe, T. Kameyama, K. Okazaki, S. Ikeda, M. Matsumura, A. Ishikawa, H. Ishihara, J. Phys. Chem. Lett. 2 (2011) 2057–2062.
[10] Y. Tian, T. Tatsuma, J. Am. Chem. Soc. 127 (2005) 7632–7637.
[11] L. Du, A. Furube, K. Yamamoto, K. Hara, R. Katoh, M. Tachiya, J. Phys. Chem. C 113 (2009) 6454–6462.
[12] H. Zhu, X. Chen, Z. Zheng, X. Ke, E. Jaatinen, J. Zhao, C. Guo, T. Xie, D. Wang, Chem. Commun. (2009) 7524–7526.
[13] S. Naya, M. Teranishi, T. Isobe, H. Tada, Chem. Commun. 46 (2010) 815–817.
[14] E. Kowalska, O.O.P. Mahaney, R. Abe, B. Ohtani, Phys. Chem. Chem. Phys. 12 (2010) 2344–2355.

[15] H. Kominami, A. Tanaka, K. Hashimoto, Appl. Catal. A 307 (2011) 121–126.
[16] A. Tanaka, K. Hashimoto, H. Kominami, Chem. Commun. 47 (2011) 10446–10448.
[17] Y. Nishijima, K. Ueno, Y. Yokota, K. Murakoshi, H. Misawa, J. Phys. Chem. Lett. 1 (2010) 2031–2036.
[18] C.G. Silva, R. Juárez, T. Marino, R. Molinari, H. García, J. Am. Chem. Soc. 133 (2011) 595–602.
[19] P. Wang, B. Huang, X. Qin, X. Zhang, Y. Dai, J. Wei, M.H. Wangbo, Angew. Chem. Int. Ed. 47 (2008) 7931–7933.
[20] R. Li, W. Chen, H. Kobayashi, C. Ma, Green Chem. 12 (2010) 212–215.
[21] B.V. Enüstün, J. Turkevich, J. Am. Chem. Soc. 85 (1963) 3317–3328.
[22] W. Patungwasa, J.H. Hodak, Mater. Chem. Phys. 108 (2008) 45–54.
[23] T. Sakata, T. Kawai, Chem. Phys. Lett. 80 (1981) 341–344.
[24] S.K. Ghosh, T. Pal, Chem. Rev. 107 (2007) 4797–4862.
[25] F. Kim, J.H. Song, P. Yang, J. Am. Chem. Soc. 124 (2002) 14316–14317.
[26] J. Zhu, L. Huang, J. Zhao, Y. Wang, Y. Zhao, L. Hao, Y. Lu, Mater. Sci. Eng. B 121 (2005) 199–203.
[27] O.O.P. Mahaney, N. Murakami, R. Abe, B. Ohtani, Chem. Lett. 38 (2009) 238–239.
[28] B. Ohtani, O.O.P. Mahaney, F. Amano, N. Murakami, R. Abe, J. Adv. Oxid. Technol. 13 (2010) 247–261.